AJEMA GLOBAL RESEARCH NETWORK

AMERICAN Journal of Engineering, Mechanics and Architecture
Volume 3, Issue 5, 2025 ISSN (E): 2993-2637

Modeling Turbulent Flow Around a Thin Rectangle Using the K–E Turbulence Model in Comsol Multiphysics

Hamdamov M.M., Muzaffarov S.A.
Institute of Mechanics and Seismic Stability of Structures of the Academy of Sciences of the Republic of Uzbekistan, Tashkent, Uzbekistan
Oriental university, Tashkent, Uzbekistan

Boborakhimova M.I.
Oriental university, Tashkent, Uzbekistan

Abstract: The article presents the results of numerical simulation of flow around a rectangular airfoil using standard Comsol solvers Multiphysics based on the k–ε turbulent model. Calculations are performed at the Reynolds number $10{,}000 < Re < 2{,}000{,}000$ and attack angles $\alpha = 0°–20°$. The dependences of the velocity distribution, pressure and other flow characteristics on the attack angle are obtained. The constructed model demonstrated good convergence, stability and high accuracy of calculations.

Keywords: k-ε model, Comsol Multiphysics, airfoil, turbulence, Reynolds number, angle of attack.

Introduction . The study of turbulent flow around bodies of various shapes is an important area of aerodynamics and fluid dynamics, which plays a key role in the design of various structures, from buildings to aircraft. Particular attention is paid to the behavior of thin rectangular profiles, since such elements are widely used in architectural structures, cooling systems, turbine blades and other technical devices that are exposed to air or fluid flows.

This paper considers the modeling of turbulent flow around a thin rectangle using the K-ε turbulence model implemented in the Comsol software environment. Multiphysics . The K-ε model is one of the most common and proven in engineering practice, allowing one to achieve an optimal balance between accuracy and computational costs when solving averaged Navier-Stokes equations based on Reynolds averaging.

The main objective of the study is to obtain flow characteristics such as velocity and pressure distribution and analysis of turbulent structure features at different Reynolds numbers and attack angles. An important aspect is also the assessment of the stability and accuracy of the proposed numerical model. The work studies the aerodynamic characteristics of a fixed wind turbine blade using a numerical solution of the Navier-Stokes equations in the RANS form, using the K-ε turbulence model. The finite volume method implemented in Comsol is used to analyze the air flow and its impact on the blade geometry Multiphysics. This approach allows for highly accurate modeling of turbulent flow behavior near a body surface and analysis of key aerodynamic parameters under various flow conditions.

Field tests , although providing high accuracy, require significant time, financial and technical costs. Analytical and semi-empirical models are often based on simplifying assumptions, which

limits their applicability in conditions of complex geometry and changing flow regimes. In this regard, the computer fluid dynamics (CFD) method is an optimal compromise between accuracy and resource costs . CFD allows detailed modeling of flow processes, obtaining complete information on the distribution of physical flow parameters without the need for expensive full-scale experiments [1-3]. The use of numerical modeling is especially important in studying the aerodynamics of wind turbine blades, where the accuracy of the prediction of force effects is critical for effective design and optimization.

There are several approaches to studying the aerodynamics of turbulent airflow around various airfoils, including field experiments, laboratory wind tunnel tests, analytical methods, and numerical modeling using CFD technologies. The latter approach demonstrates high potential due to the ability to analyze complex geometries and flow regimes at reasonable computational costs.

A two-dimensional problem of a flat plate of length flowing past $c = 1\ m$ a turbulent uniform flow is considered. The geometry of the flow calculation region is shown in Fig. 1. It is assumed that the plate has a stationary motionless position. The boundary in the form of a semicircle is taken as the boundary of the unperturbed flow at admissible values of the angle of attack of the plate by the flow. The center of the semicircle with a radius of 20 m is located in the same place $(0.5;0)$ – at the bottom edge of the plate.

In the context of the wind turbine aerodynamics developed within the framework of this study, the relevance of the problem lies in determining the aerodynamic forces - the drag force and the lift force acting on a separate working element of a vertical-axis wind turbine (VAWT) when flowing around it by an air stream at different angles of attack. These forces are critically important for analyzing the efficiency of converting the kinetic energy of the wind into the mechanical energy of rotor rotation.

The working elements of the wind turbine under study are thin flat rectangular plates fixed in a certain position on the frame. In the operating mode, they are fixed at an angle that facilitates the generation of useful torque, and in the non-operating mode, they are oriented neutrally in the direction of the flow, minimizing resistance.

The formulation of this problem differs significantly from the classical problem of uniform laminar flow around a flat plate. Firstly, this study considers the turbulent flow regime, which is typical for most wind turbine operating conditions. Secondly, the geometry of the streamlined surface is limited in length, which affects the formation of the boundary layer and the pressure distribution. These features require the use of a numerical approach using a reliable turbulence model, such as k-ε, and high-precision discretization of the computational domain.

In this regard, the formulation of the problem is new, since it takes into account the effect of the presence of a second edge of the plate.

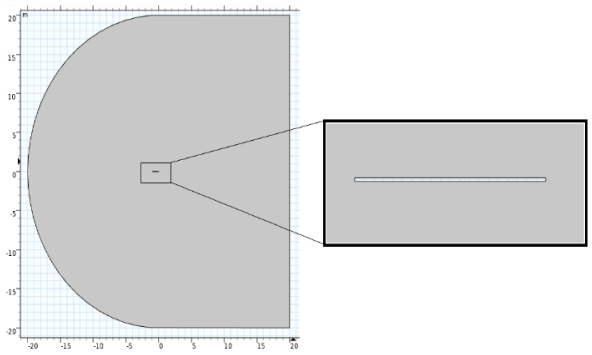

Fig. 1. Geometry of the flow region around the plates

Boundary conditions on the semicircle and on the boundaries $y = \pm 20\ m$ (on the boundary G_1) are set depending on the angle of attack

$$U(x_{G1}, y_{G1}) = U_0 \cos\alpha, \quad V(x_{G1}, y_{G1}) = U_0 \sin\alpha \qquad (1)$$

where U $_0$ is the modulus of the velocity of the flow incident on the main flow a ; α – the angle between the direction of flow and the coordinate axis *OX* .

At this boundary, the excess pressure value is zero .

$$P(x_{G1}, y_{G1}) = 0 \ \ (Pa).$$

The plate in the computational domain is represented by thickness 0.8 mm and 1 m long. Accordingly, for

$$G_2 = \left\{ \left[\left(x = 0 \cup x = 1, \cap |y| \le 0.004 \right) \right] \cup \left[\left(y = \pm 0.004 m \right) \cap \left(0\ m \le x \le 1m \right), \right] \right\}$$

set the conditions $U(x_{G2}, y_{G2}) = V(x_{G2}, y_{G2}) = 0\ m/s.$

At the exit from the calculation region $y = 20\ m$ (G_3) to determine the velocities, the condition of smooth conjugation was adopted

$$\frac{\partial U(x_{G3}, y_{G3})}{\partial n} = 0, \frac{\partial V(x_{G3}, y_{G3})}{\partial n} = 0$$

The establishment of an incompressible fluid flow is considered. As the establishment parameter, *t* can be taken, due to which the two-dimensional Nave -Stokes equations are taken in the form [4-5].

$$\begin{cases} \dfrac{\partial \rho}{\partial t} + \dfrac{\partial \rho U}{\partial x} + \dfrac{\partial \rho V}{\partial y} = 0, \\ \dfrac{\partial \rho U}{\partial t} + \dfrac{\partial \rho UU}{\partial x} + \dfrac{\partial \rho UV}{\partial y} + \dfrac{\partial p}{\partial x} = \dfrac{\partial}{\partial x}\left(\mu_{eff} S_{11}\right) + \dfrac{\partial}{\partial y}\left(\mu_{eff} S_{12}\right), \\ \dfrac{\partial \rho V}{\partial t} + \dfrac{\partial \rho UV}{\partial x} + \dfrac{\partial \rho VV}{\partial y} + \dfrac{\partial p}{\partial y} = \dfrac{\partial}{\partial x}\left(\mu_{eff} S_{12}\right) + \dfrac{\partial}{\partial y}\left(\mu_{eff} S_{22}\right). \end{cases} \qquad (2)$$

Here

$$S_{11} = 2\frac{\partial U}{\partial x} - \frac{2}{3}\left(\frac{\partial U}{\partial x} + \frac{\partial U}{\partial y}\right); \qquad S_{12} = \frac{\partial U}{\partial y} + \frac{\partial V}{\partial x};$$

$$S_{22} = 2\frac{\partial V}{\partial y} - \frac{2}{3}\left(\frac{\partial U}{\partial x} + \frac{\partial V}{\partial y}\right); \qquad \mu_{eff} = \mu + \mu_t.$$

The second and third equations of system (2) are used in the formulation of the problem for the pressure on the boundary G_2 , which are of the second kind and take into account the boundary values of the velocities on this boundary.

Closing the system (2) requires the use of the equation of state of a perfect gas [6-8]

$$p = \rho RT$$

where *R* is the reduced gas state of air ; *T=293.15* - air temperature, and determining the value of effective viscosity μ_{eff} .

For the considered variants of the problem, the Reynolds number was

$$\mathrm{Re}=\frac{\rho u_0 l}{\mu}=\frac{1.2043\times 20\times 1}{1.81397\times 10^{-5}}=1.327805\times 10^{6},$$

which corresponds to the developed regime of turbulent flow around a solid surface. That is, in the calculations we $\mu=1.81397*10^{-5}\frac{kg}{m\cdot s}$ took and . In accordance with this, the turbulence model is selected .

A modified turbulence model was chosen as the model $k-\varepsilon$ model [9-11]:

$$\begin{cases}\dfrac{\partial\rho k}{\partial t}+U\dfrac{\partial\rho k}{\partial x}+V\dfrac{\partial\rho k}{\partial y}=\dfrac{\partial}{\partial x}\left[\left(\mu+\dfrac{\mu_t}{\delta_k}\right)\dfrac{\partial k}{\partial x}\right]+\dfrac{\partial}{\partial y}\left[\left(\mu+\dfrac{\mu_t}{\delta_k}\right)\dfrac{\partial k}{\partial y}\right]+\\ +G_k+G_b-\rho\varepsilon-2\rho\varepsilon M_t^2+S_k;\\ \dfrac{\partial\rho\varepsilon}{\partial t}+U\dfrac{\partial\rho\varepsilon}{\partial x}+V\dfrac{\partial\rho\varepsilon}{\partial y}=\dfrac{\partial}{\partial x}\left[\left(\mu+\dfrac{\mu_t}{\delta_\varepsilon}\right)\dfrac{\partial\varepsilon}{\partial x}\right]+\dfrac{\partial}{\partial y}\left[\left(\mu+\dfrac{\mu_t}{\delta_\varepsilon}\right)\dfrac{\partial\varepsilon}{\partial y}\right]+\\ +\rho C_1 S\varepsilon-\rho C_2\dfrac{\varepsilon^2}{k+\sqrt{\upsilon\varepsilon}}+C_{1\varepsilon}\dfrac{\varepsilon}{k}C_{3\varepsilon}G_b+S_\varepsilon,\end{cases}\qquad(3)$$

which contributes to a more adequate description of heat and mass transfer processes. The following notations are used here

$$C_1=\max\left[0.43,\frac{\eta}{\eta+5}\right],\quad \eta=S\frac{k}{\varepsilon},\quad S=\sqrt{2S_{ij}S_{ij}},\quad \mu_t=\rho C_\mu\frac{k^2}{\varepsilon},\quad C_\mu=\frac{1}{A_0+A_S\dfrac{kU^*}{\varepsilon}},$$

$$U^*\equiv\sqrt{S_{ij}S_{ij}+\tilde{\Omega}_{ij}\tilde{\Omega}_{ij}},\quad \Omega_{ij}=\overline{\Omega_{ij}}-2\varepsilon_{ijk}\omega_k,\quad A_S=\sqrt{6}\cos\phi,\quad \phi=\frac{1}{3}\cos^{-1}\left(\sqrt{6}W\right),\quad W=\frac{S_{ij}S_{jk}S_{ki}}{\tilde{S}^3},$$

$$\tilde{S}=\sqrt{S_{ij}S_{ij}},\quad S_{ij}=\frac{1}{2}\left(\frac{\partial u_j}{\partial x_i}+\frac{\partial u_i}{\partial x_j}\right),\quad G_k=-\rho\overline{u_i'u_j'}\frac{\partial u_j}{\partial u_i},\quad S\equiv\sqrt{2S_{ij}S_{ij}},\quad G_b=\beta g_i\frac{\mu_t\partial T}{\mathrm{Pr}_t\partial x_i},$$

$$a_0=1/\mathrm{Pr}=k/\mu c_p,\ \beta=-\frac{1}{\rho}\left(\frac{\partial\rho}{\partial T}\right)_p,\ G_b=-g_i\frac{\mu_t}{\rho\,\mathrm{Pr}_t}\frac{\partial\rho}{\partial x_i},M_t=\sqrt{\frac{k}{a^2}}\ \mathrm{Pr}_t=1/a_t\ a=\sqrt{\gamma RT}.$$

The empirical constants $k-\varepsilon$ of the model take standard values: $C_{1\varepsilon}=1.44$, $C_2=1.9$, $\sigma_k=1.0$, $\sigma_\varepsilon=1.2$, $A_0=4.04$.

Model $k-\varepsilon$ is indeed one of the most popular and widely used models of first-level turbulence. It is based on two main variables: the density of turbulent kinetic energy (k) and the rate of dissipation of this energy (ε). This model uses two nonlinear diffusion equations to calculate turbulent quantities, which allows it to more accurately describe the behavior of turbulent flows under various conditions.

Considering that the selected turbulence model is included in the list of implemented turbulence models Comsol Multiphysics, then the calculations were carried out in this environment.

Calculations were carried out for 10000< Re < 2000000 for different angle of attack options from the interval $0^0\le\alpha\le 20^0$

The calculations used local grid thickening near the surface of the profile shown in Fig. 2.

60,200 elements is used for the flow region around the profile . Standard no-slip boundary conditions at the walls and extrapolation conditions at the outlet are used in equations (2).

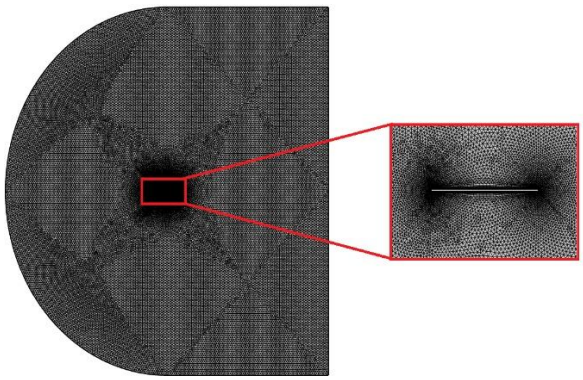

Fig. 2. Calculation grid of the profile flow

The initial data for calculating the parameters were the following values: wind speed in m/s, angular velocity in rad/s, air density in kg/m³ and pressure in Pa (see Fig. 3).

Label: Parameters 1

Parameters

Name	Expression	Value	Description
U_inf	20[m*s^-1]	20 m/s	Free-stream velocity
rho_inf	1.2043[kg*m^-3]	1.2043 kg/m³	Free-stream density
mu_inf	1.81397e-5[kg*m^-1*s^-1]	1.814E-5 kg/(...	Free-stream dynamic vis...
L	20[m]	20 m	Domain reference length
c	1[m]	1 m	Chord length
k_inf	0.1*mu_inf*U_inf/(rho_inf*L)	1.5062E-6 m²/s²	Free-stream turbulent kin...
om_inf	10*U_inf/L	10 1/s	Free-stream specific dissi...
alpha	0	0	Angle of attack
Re	U_inf*c*rho_inf/mu_inf	1.3278E6	

Fig. 3. Initial data window with dimensions and initial values

The establishment method was used to solve the problem. The results of potential flow were used as an initial approximation. The principle of the program on finite volumes is that the velocity fields are first determined for a fixed time. They are used to determine the pressure increments, relative to which the Poisson equation is compiled .

On average, the program worked for two or more hours. The results were longitudinal and transverse velocity fields, pressure fields, kinematic energy of turbulence and its dissipation.

Also of practical interest are the local coefficients of friction force and aerodynamic forces acting on the plate.

As calculations have shown, at small angles of attack the lifting force increases almost linearly with respect to the angle of attack. But after that a non-monotonic nature of the change in lifting force is observed. Accordingly, it can be assumed that the force acting on the wind generator blades will have a periodic nature, and the maximum force of the air flow acts at small deviations of the blade position from the flow direction.

The obtained results differ significantly from the results of flow around an infinite plate, since significant gradients of the object's parameters are observed both at the leading and trailing edges of the plate.

Time-averaged longitudinal velocity (or flow velocity) profiles allow us to estimate the flow characteristics at different points near and after the profile. In our case, the longitudinal velocity and pressure graphs are estimated in five sections x/c = 0, 0.25, 0.5, 0.75, and 1 m.

Figure 4 shows the graphs of the longitudinal velocity in the listed sections at the values of the angle of attack $\alpha = 2^\circ, 6^\circ, 10^\circ, 14^\circ, 18^\circ, 20^\circ$. The undisturbed flow velocity was 20 m/s, and the Reynolds number was 1,327,800.

Pressure field

The following figure shows the isobar field at $\alpha = 2^\circ$.

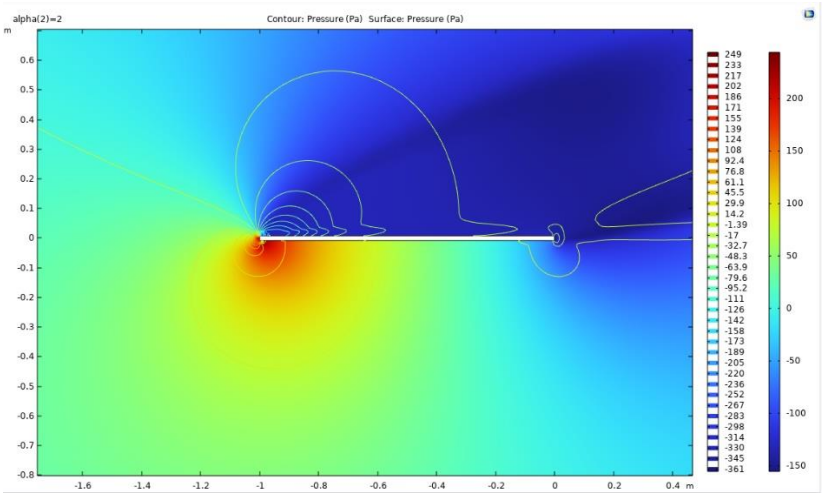

Fig.4. Pressure field at $\alpha = 2^\circ$

The highest pressure was 265.5 Pa at the wing angle of attack $\alpha = 2^\circ$. In the figure it is highlighted in red and formed at the input tip of the wing. The lowest pressure was -240.1 Pa.

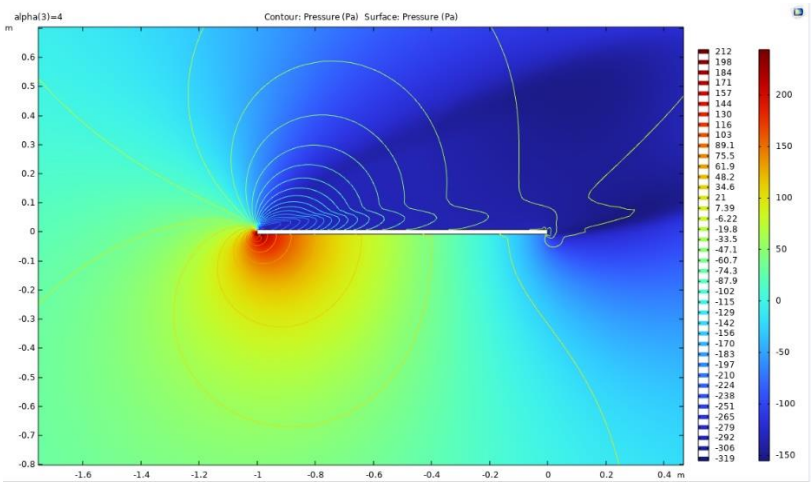

Fig.5. Pressure field at $\alpha = 4^\circ$

Fig. 5 shows the pressure field at $\alpha = 4^\circ$. On the side washed by the direct flow (lower part of the graph) the pressure increased. The highest pressure was formed on the wing tip (highlighted in red) and it was equal to 211.6 Pa. The lowest pressure was formed on the leeward side and was – 319.4 Pa (the pressure on the incoming flow was taken to be zero).

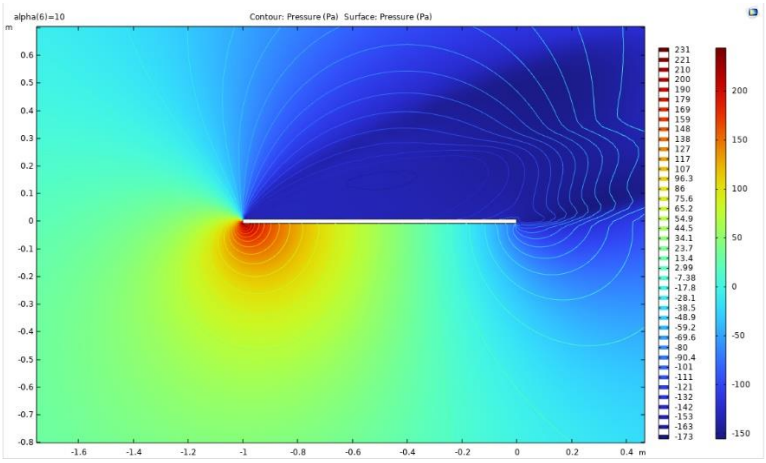

Fig.6. Pressure field at $\alpha = 10^{\circ}$

In relation to the previous case, $\alpha = 10^{\circ}$ both the highest and lowest pressures increased . In particular, the highest pressure was 231.2 Pa, and the lowest pressure was 173.3 Pa.

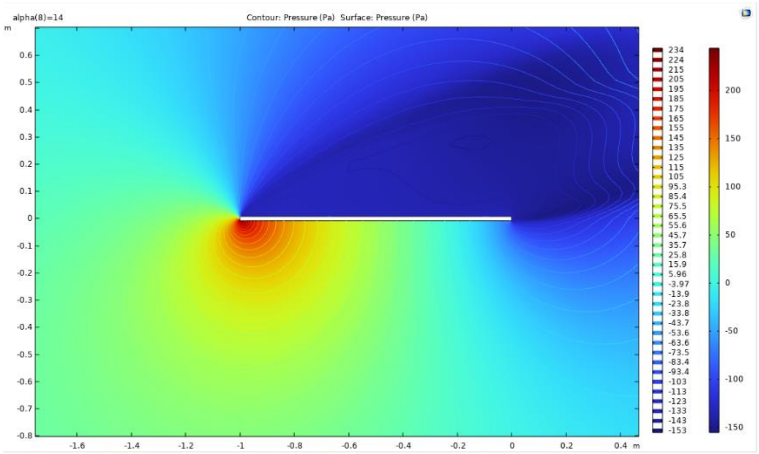

Fig. 7. Pressure field at $\alpha = 14^{\circ}$

In relation to the previous case, $\alpha = 10^{\circ}$ at The values of the highest and lowest pressure $\alpha = 14^{\circ}$ also increased, amounting to 234.4 and –152.9 Pa, respectively.

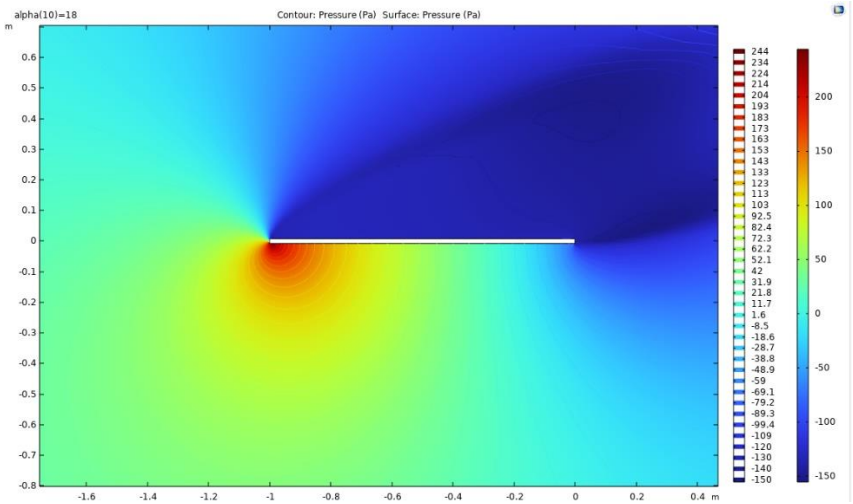

Fig.8. Pressure field at $\alpha = 18^{\circ}$

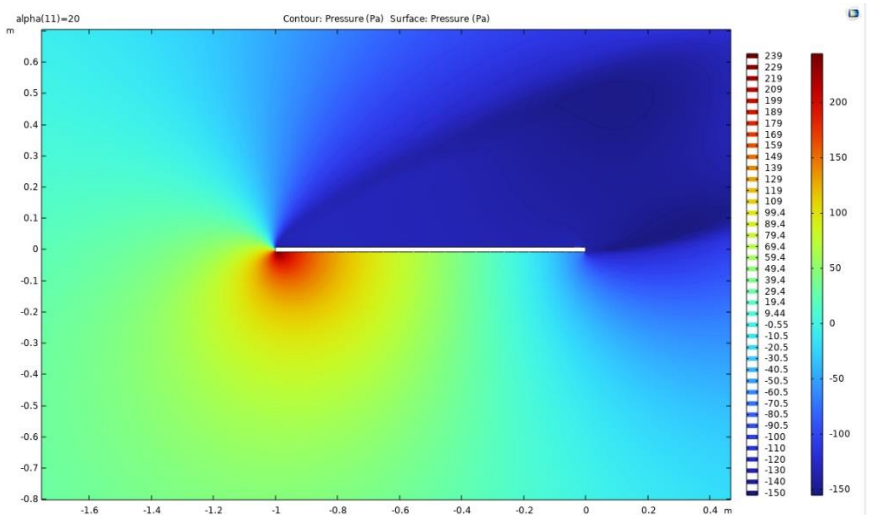

Fig . 9. Pressure field at $\alpha = 20^{\circ}$

The highest pressure was 244 Pa at $\alpha = 18^{\circ}$ the wing (Fig. 8), and the lowest pressure was – 149.9 Pa. And at $\alpha = 20^{\circ}$ (Fig. 9) these figures were 239.2 Pa and – 150.4 Pa, respectively.

Change in pressure on the plate surfaces

The distribution of the surface pressure coefficient (in some sources this value is called the cavitation coefficient) on the wing surface is characterized by the change in pressure on its surface depending on the distance from a certain point. Usually, the surface pressure coefficient (C_p) is used in the analysis, which is defined as the ratio of the pressure difference between a point on the profile surface and the free flow pressure to the dynamic pressure of the free flow:

$$C_p = \frac{p - p_\infty}{0.5\rho U_0^2},$$

Where p is the pressure at a point on the profile surface; p_∞ is the pressure of the incoming flow; ρ is the density of the medium; U_0 is the velocity of the incoming flow.

C_p graphs usually distinguish between positive and negative pressure zones. The positive pressure zone is usually called the lift zone, and the negative pressure zone is called the drag zone. The distribution of the surface pressure coefficient on the wing profile can be used to analyze its aerodynamic characteristics, such as lift, drag coefficient, etc.

Fig. 10 shows the values of the surface pressure coefficient C_p on the leeward and windward sides of the streamlined plate at angles of attack $\alpha = 0^{\circ}$, 4°, 8°, 12°, 16° and 20°.

At an angle of attack $\alpha = 0^{\circ}$ when the flow is incoming, there is first a sudden increase in the value of C_p over 1, and then a sharp decrease to 1. This corresponds to the fact that at the edge of the plate the flow is slowed down, which causes a sudden increase in pressure. Then the flow is divided into two equal parts and accelerates - this explains the sudden decrease in pressure. Then the pressure value is close to the pressure of the incoming flow.

Note that in the experimental study of flow around a plate, the edge is given a wedge shape. This method usually eliminates pressure surges near the edge of the plate [8]. Otherwise, these pressure surges can lead to the formation of vortices of different scales and early turbulence of the flow when flowing around the plate.

In a similar way, but different flow distributions when flowing around a plate can explain the behavior of the pressure on the windward and leeward sides of the plate being flown around, depending on the angle of attack α (Fig. 10) . The general tendency of the change in the value of

the surface pressure coefficient C_p repeats what was noted in the analysis of the highest and lowest values of pressure around the plate.

The distribution of the coefficient of surface friction on an aerodynamic profile is characterized by a change in the friction force on its surface depending on the distance from a certain point.

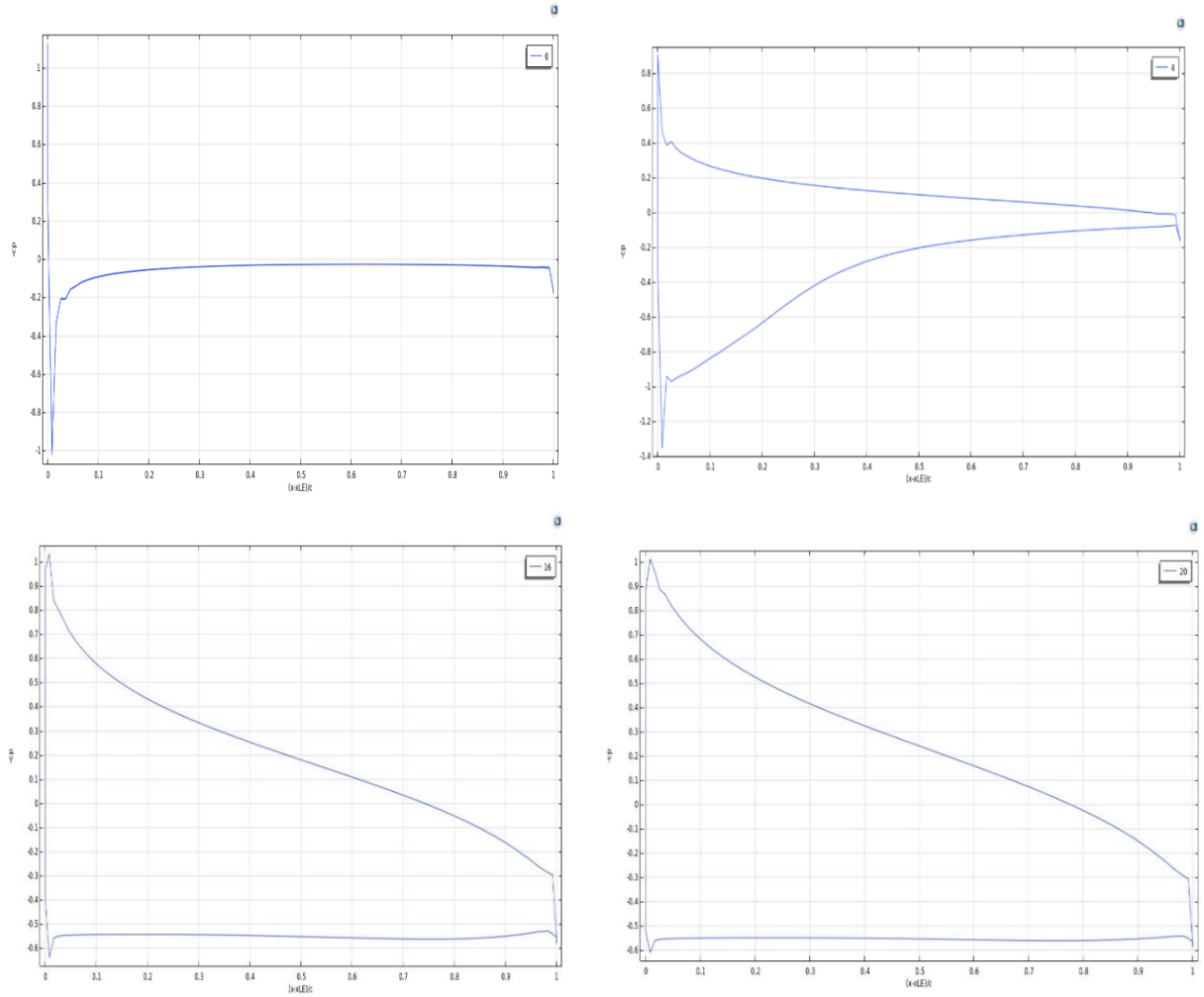

Fig.10 . Surface pressure coefficient C_p

The coefficient of surface friction C_f is defined as the ratio of the friction force acting on the surface of the profile to the dynamic pressure of the free flow [12,13]:

$$C_f = \frac{F}{0.5\rho U_0^2 S},$$

Where F is the friction force acting on the profile surface; S is the profile surface area oriented along the flow.

To analyze the distribution of the surface friction coefficient on a wing profile, graphs of C_f *are usually used* depending on the distance from a certain point on the profile surface. The graphs of C_f also usually distinguish zones of increased and decreased friction. The zone of increased friction is usually located in the area of the leading edge of the profile and in the area of flow separation on the upper surface of the profile, as can be seen in Fig. 11.

As can be seen from the graphs, the main changes in the coefficient of surface friction on the wing profile occur at the edges of the plate. In the calculation results, it turned out to be non-monotonic. This can be explained by the presence of a large gradient of indicators near the edge of the plate and not a very adequate choice of the step of the numerical solution of the problem.

But peculiar distributions of this value are observed in the windward and leeward surfaces of the plate.

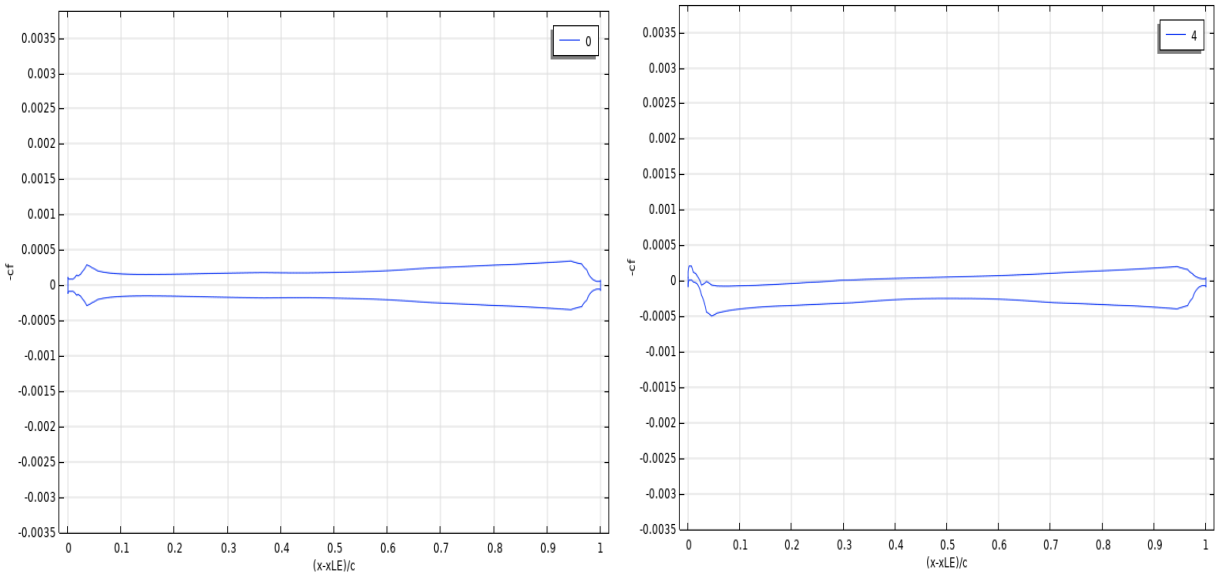

Fig.11. Surface friction coefficient C_f

In Fig. 12, the changes in the kinetic energy of turbulence along the vertical coordinate are presented in various sections. They demonstrate the features of the flow turbulization depending on the angle of attack α. It is noticeable that downstream, starting from zero, it increases intensively in the plate zone and decreases after the plate. The greatest value of the kinetic energy of turbulence moves upward.

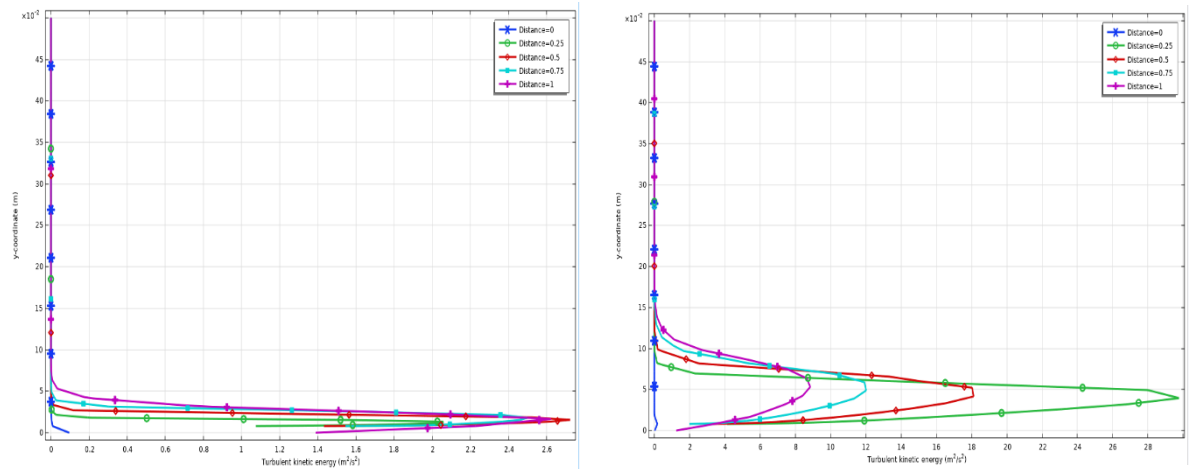

$\alpha = 0^\circ$ $\alpha = 4^\circ$

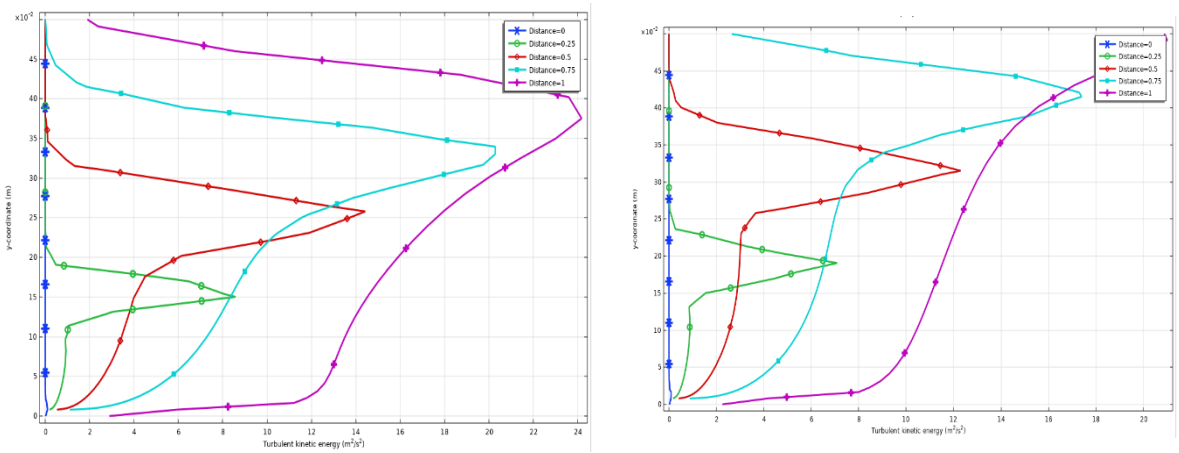

$\alpha = 16^{\circ}$ $\alpha = 20^{\circ}$

Fig.12 . Kinetic energy of turbulence in different sections

The dissipation of turbulence energy (Fig.13) with its character of convective transfer repeats the material presented above.

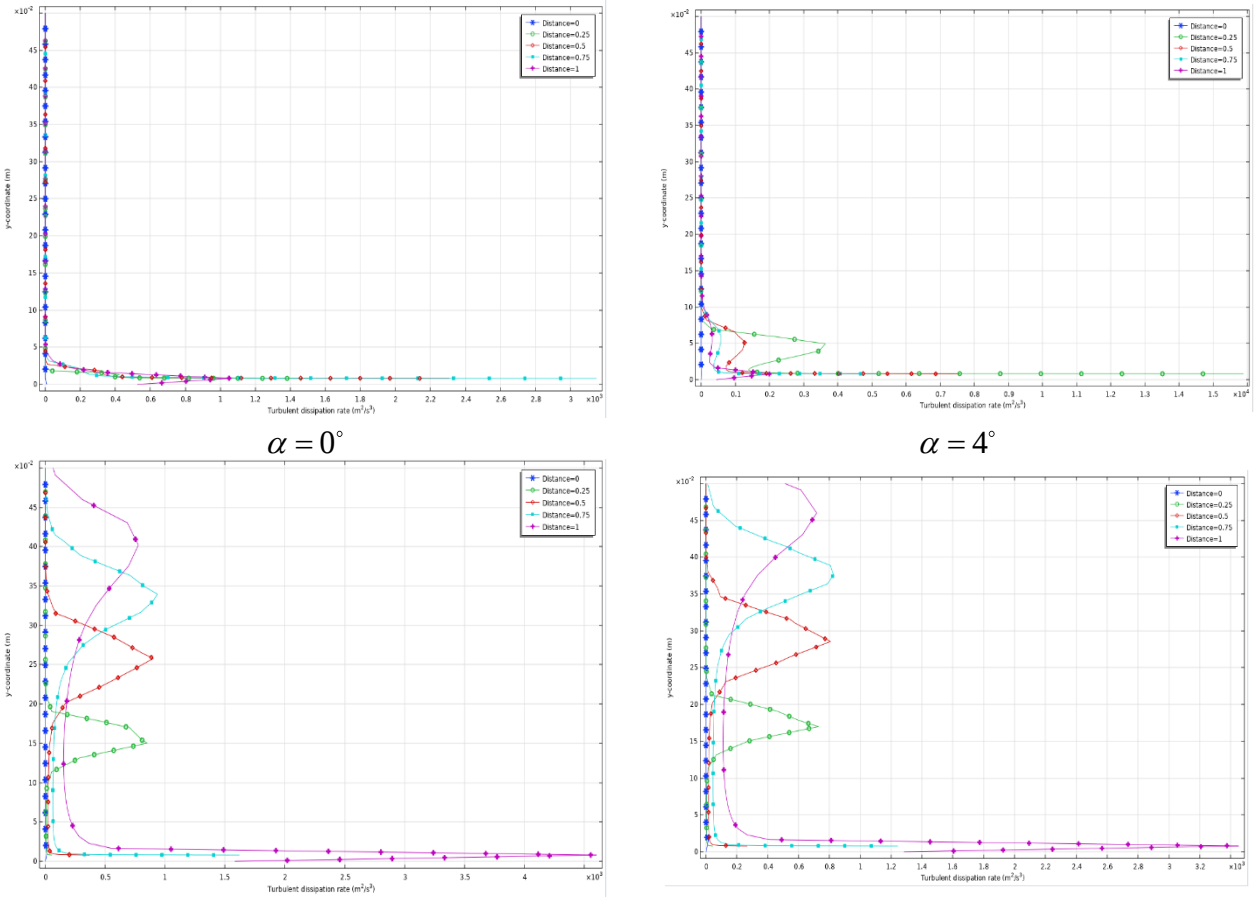

$\alpha = 0^{\circ}$ $\alpha = 4^{\circ}$

$\alpha = 16^{\circ}$ $\alpha = 20^{\circ}$

Fig. 13 . Dissipation of turbulent energy in different sections

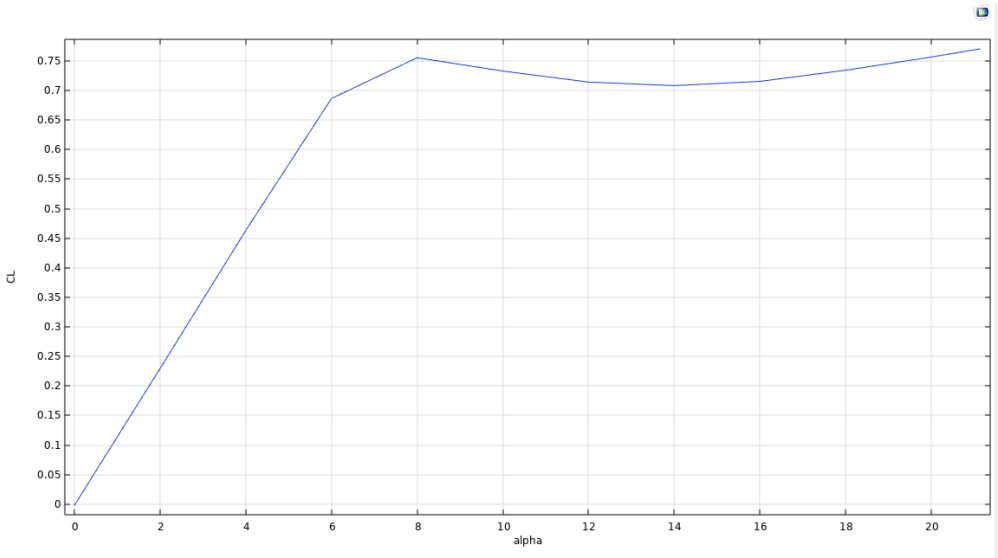

Fig. 14. Effect of angles of attack on lift coefficients.

The last figure 15 shows the graphs of the longitudinal velocity along the same coordinate in the plane that passes through the leading edge of the streamlined plate at different angles of attack. At $\alpha \succ 0^{\circ}$ near the leading edge, a section with negative velocity (flow reversal) is formed. Only

after this does the longitudinal velocity begin to grow. With an increase in the angle of attack, moving away from the inlet section, the greatest value of the longitudinal velocity increases.

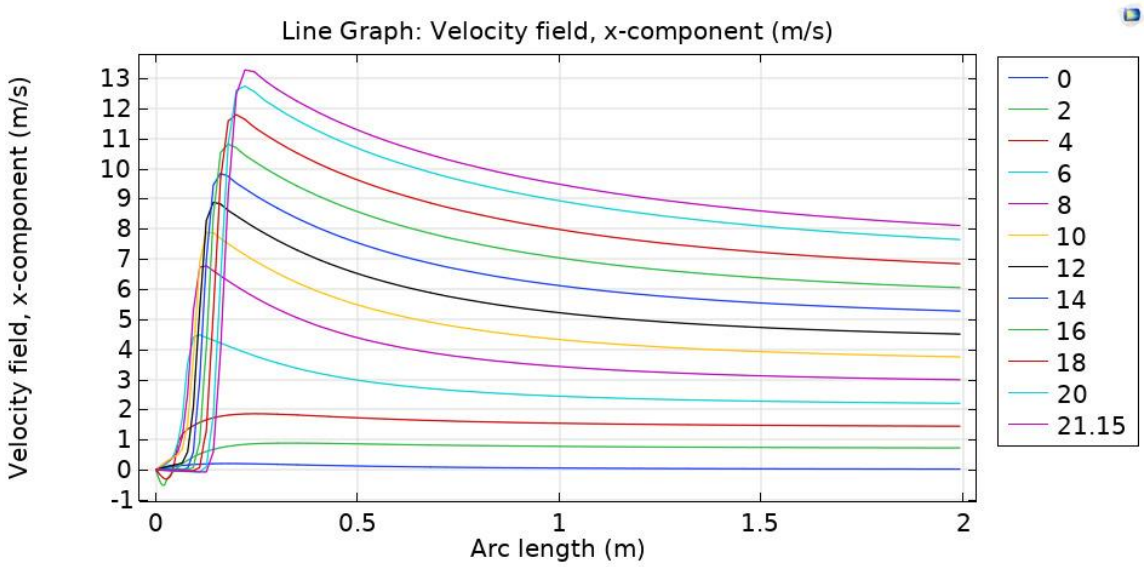

Fig.15. Velocity field for different values α

Conclusion. The paper presents numerical results of turbulent two-dimensional flow of an incompressible fluid around a stationary rectangle profile using $k-\varepsilon$ turbulence models in the Comsol software package Multiphysics .

At different angles of attack, the fields of longitudinal and transverse flow velocities, pressure, kinetic energy of turbulence and its dissipation, as well as information on the surface pressure coefficient (cavitation coefficient) on the wing profile, as well as the surface friction coefficient, were obtained and analyzed.

The results of turbulent flow around a flat plate at three different angles of attack showed significant differences from the results of flow around an infinite plate, since when flowing around a plate of finite length, the influence of both the leading and trailing edges of the plate is observed.

The results obtained at a flow velocity of 20 m/s, a plate length of 1 m and at small angles of attack ($0^\circ \le \alpha \le 20^\circ$) showed that with an increase in the angle of attack, a non-monotonic velocity profile is formed on the leeward side of the profile with an increase in the maximum value of the velocity vector modulus. The resulting braking zones at the leading and trailing edges of the plate spread wider and wider with an increase in the angle of attack.

LITERATURE

1. Orozco Murillo, W., Palacio- Fernande , JA, Patiño Arcila , ID, Zapata Monsalve , JS, & Hincapie Isaza , J. A. (2020). Analysis of a Jet Pump Performance under Different Primary Nozzle Positions and Inlet Pressures using two Approaches: One Dimensional Analytical Model and Three Dimensional CFD Simulations. Journal of Applied and Computational Mechanics, 6(Special Issue), 1228-1244.
2. Hadad , K., Eidi , H. R., & Mokhtari , J. (2017). VOC level control by ventilation improvement of Flexography printing room using CFD modeling. Journal of Applied and Computational Mechanics, 3(3), 171-177.
3. Tsega , E. G., & Katiyar , V. K. (2019). A Numerical Simulation of Inspiratory Airflow in Human Airways during Exercise at Sea Level and at High Altitude. Journal of Applied and s